Journal of Catalysis 279 (2011) 352–360

Contents lists available at ScienceDirect

Journal of Catalysis

journal homepage: www.elsevier.com/locate/jcat

Interaction of SO_2 with Cu/TiC(0 0 1) and Au/TiC(0 0 1): Toward a new family of $DeSO_x$ catalysts

Leticia Feria [a], José A. Rodriguez [b], Tomas Jirsak [b], Francesc Illas [a,*]

[a] Department de Química Física & Institut de Química Teòrica i Computacional (IQTCUB), Universitat de Barcelona, C/ Martí i Franquès 1, 08028 Barcelona, Spain
[b] Chemistry Department, Brookhaven National Laboratory, Upton, NY 11973, USA

ARTICLE INFO

Article history:
Received 15 November 2010
Revised 4 January 2011
Accepted 9 February 2011
Available online 11 March 2011

Keywords:
$DeSO_x$
Au nanoparticles
Cu nanoparticles
TiC
XPS
DFT

ABSTRACT

Experiments carried out under well-controlled conditions and density functional theory (DFT)-based calculations evidence that Cu and Au nanoparticles supported on a TiC(0 0 1) surface are quite active for the dissociation of the SO_2 molecule. The Cu/TiC(0 0 1) and Au/TiC(0 0 1) systems cleave both S–O bonds of SO_2 at a temperature of 150 K, displaying a reactivity much larger than that of TiC(0 0 1) or extended surfaces of bulk copper and gold. The origin of the high activity of the Cu/TiC(0 0 1) and Au/TiC(0 0 1) systems lies on the interaction between the C atoms of the substrate and the metal atoms of the supported particle, which results in a large polarization of its electron density. Experiments and theory consistently indicate that the Cu/TiC system is more active toward SO_2 dissociation than the Au/TiC system. This type of systems may provide alternative and efficient $DeSO_x$ catalysts.

1. Introduction

There is a continuous demand for the reduction of toxic emissions from the combustion of fossil fuels [1]. Sulfur dioxide (SO_2) is a major air pollutant involved in the formation of smog and acid rain [1–3]. SO_2 is frequently formed during the combustion of fossil-derived fuels in factories, power plants, houses, and automobiles [1,3a]. In general, sulfur species in the form of organo-sulfur compounds are present in gasoline and other fuels [4]. In the typical engine exhaust, 5–20 ppm of SO_2 is formed after combustion and, apart from environmental damage, SO_2 poisons the catalysts used in the automotive catalytic converters [1–3]. Furthermore, in oil refineries, large quantities of SO_2 gas are produced during the regeneration of reforming catalysts [2,4]. In the catalytic reforming of petroleum, the catalysts are deactivated by the deposition of coke residues that contain sulfur and are usually removed by burning in air with concomitant increase in environmental problems [2,4]. Every year, the negative effects of acid rain (main product of the oxidation of SO_2 in the atmosphere) on the ecology and corrosion of monuments or buildings are tremendous [1,3a]. Thus, there is a continuous search for catalysts or sorbents that have a high efficiency for the destruction or removal of SO_2 [2,3,5].

In this article, we investigate the adsorption and decomposition of SO_2 on Cu/TiC(0 0 1) and Au/TiC(0 0 1) surfaces. Metal carbides have been cited as useful materials for desulfurization reactions [6,7]. It is well known that Au(1 1 1)- and Au-extended surfaces interact weakly with SO_2 and are not efficient for the dissociation of S–O bonds [8]. However, it has been recently shown that Au ↔ carbide interactions can enhance the chemical activity of gold toward SO_2 and thiophene dissociation when deposited in the form of small, preferentially flat, nanoparticles [9,10]. Nevertheless, the high cost of Au prevents the use of this type of systems in large-scale industrial applications. On the other hand, Cu is much cheaper and Cu on TiC could be a better candidate as potential catalysts. In fact, copper supported on zeolites, ceria and alumina is a catalyst for the Claus reaction ($SO_2 + 2H_2S \rightarrow 3S + 2H_2O$) and for the reduction of sulfur dioxide by CO ($SO_2 + 2CO \rightarrow 2CO_2 + S$) [2,11]. It is not completely clear how these interesting systems operate at a microscopic or molecular level. From previous studies, it is known that SO_2 dissociates on Cu(1 0 0) and Cu(1 1 1) [12–16]. On these surfaces, the molecule adsorbs intact at 100 K and undergoes decomposition at temperatures between 200 and 300 K. The final products of the decomposition process are S and O adatoms with SO_3 as an intermediate. SO_3 could be the result of a $3SO_2 \rightarrow 2SO_3 + S$ disproportionation reaction [13,15,16]. The formation of SO as a stable intermediate during the decomposition of SO_2 on copper surfaces was postulated on the basis of photoemission data, [17] but this view has been challenged by the results of subsequent NEXAFS experiments [15]. Thermochemical data estimates derived from a semi-empirical bond-order conservation Morse-potential formalism (BOC-MP)

* Corresponding author. Fax: +34 93 402 1231.
E-mail address: francesc.illas@ub.edu (F. Illas).

0021-9517/$ - see front matter © 2011 Elsevier Inc. All rights reserved.
doi:10.1016/j.jcat.2011.02.004

suggest that SO is not viable as a stable intermediate during the decomposition of SO_2 on copper substrates [18]. Moreover, the results of density functional theory (DFT)-based calculations indicate that, from a thermochemical viewpoint, it is much easier to generate SO_3 than to form SO during the decomposition of sulfur dioxide on Cu(1 0 0) [16].

In this study, our photoemission and DFT results indicate that small nanoparticles of Cu and Au in contact with TiC(0 0 1) are highly active for the destruction of SO_2. These systems display a behavior quite different from those seen for the interaction of SO_2 with TiC(0 0 1) [19] or with extended surfaces of copper [12–17] and gold [8] The bonding of the admetals to TiC(0 0 1) induces electronic perturbations that enhance their ability to cleave S–O bonds. These phenomena are not seen on oxide supports frequently used for $DeSO_x$ processes [2], stressing the unique role of the metal carbide surface and pointing toward a new family of systems (Cu/TiC and Au/TiC) with potential use in industry and other technological applications.

2. Experimental and theoretical methods

2.1. Photoemission experiments

In section III, we will describe the results of a series of photoemission experiments performed in a ultra-high vacuum chamber (base pressure $\sim 6 \times 10^{-10}$ Torr) that is part of the U7A beamline of the National Synchrotron Light Source (NSLS) at Brookhaven National Laboratory (BNL) [5,10,19]. This ultra-high vacuum (UHV) chamber contains a hemispherical electron energy analyzer with multichannel detection, instrumentation for low-energy electron diffraction (LEED), a quadrupole mass spectrometer, and a dual anode Mg/Al Kα X-ray source. The S 2p, Au 4f and C 1s spectra were taken using a photon energy of 380 eV, whereas a photon energy of 625 eV was used to collect the O 1s data. The overall instrumental resolution in the photoemission studies was ~0.35 eV. In regular XPS experiments, Mg K radiation was used to record the core-level spectra (Cu 2p, O 1s, Ti 2p, C 1s, S 2p, Au 4f regions) and the resolution was in the range of 0.8–1.0 eV. This resolution is adequate since conventional XPS was mainly used to follow the deposition of atomic sulfur on the surfaces, and the S 2p features for this species appear well separated from those of adsorbed SO_x groups [5,19].

The TiC(0 0 1) single crystal was cleaned following methodologies reported in the literature [7b,9,20]. Copper and gold were vapor-deposited on the TiC(0 0 1) surface at 300 K. The Cu or Au doser consisted of a resistively heated W basket with a drop of ultrapure Cu or Au inside [21]. Initially, the flux of each doser was calibrated by taking thermal desorption spectra for the desorption of Cu or Au from a Mo(1 0 0) substrate [21,22]. This information was then used to calibrate admetal coverages estimated by means of photoemission or XPS. SO_2 (99.98% purity, Mattheson) was dosed to the admetal/carbide surfaces at 150 K or 300 K using capillary dosers. The reported SO_2 exposures are uncorrected for enhancement factors.

Before closing this section, we would like to add that cluster size distribution for Au [9,10] and Cu nanoparticles supported on TiC(0 0 1) has been determined from STM experiments. These experiments show that for small loadings of the admetals, a condition that leads to an extremely high chemical activity as we show below, the majority of particles are small and flat. This information is crucial and has obvious implications for the design of appropriate models. With respect to the Cu/TiC system, for comparative purposes, it is assumed that the morphology of the supported Cu particles is similar to that of the Au clusters used in previous studies [9,10], and this is used in the models as described in the next section.

2.2. First-principles density functional calculations

The adsorption of SO_2 on Cu/TiC(0 0 1) and Au/TiC(0 0 1) model systems was also studied by means of calculations based on density functional theory, within the usual Kohn–Sham formalism, carried out for suitable periodic representations of these systems. The Perdew–Wang functional (PW91) of the generalized gradient approximation (GGA) has been chosen for the exchange–correlation potential [23]. The effect of the atomic cores on the valence electron density has been taken into account by means of the projected augmented plane-wave (PAW) method of Blöchl [24] as implemented by Kresse and Joubert [25] in the VASP code [26,27]. This representation of the core states allows one to obtain converged results with a cutoff kinetic energy of 415 eV for the plane-wave basis set. The Monkhorst–Pack scheme [28] has been used to select the special k points used to carry out the numerical integrations in the reciprocal space. A conjugated gradient algorithm with an energy criterion of 0.001 eV has been used for the atomic convergence, ensured forces to be in all cases smaller than 0.03 eV/Å.

The TiC(0 0 1) surface has been represented by slab models repeated periodically with a vacuum region of 10 Å between repeated slabs. The slabs were constructed using the lattice parameter optimized for the bulk of TiC and reported in a previous work [29]. They all contained four atomic layers but different surface area. In all cases, the two outermost layers of one side of the slab were completely allowed to relax. Cu_4 and Au_4 clusters or Cu and Au monolayers were set above the TiC(0 0 1) surface, and the vacuum space enlarged accordingly to maintain the repeated slabs enough away from each other [9,10]. The metal adatoms were placed initially above C atoms [9,10]. The structure of the supported particles and monolayers was always fully optimized allowing the two uppermost atomic layers of the TiC substrate to relax. This type of geometry optimization was also carried out in the series of calculations where the SO_2 molecule interacts with the supported Cu and Au systems.

For supported Cu_4 and Au_4, we used a 3×3 unit cell (144 + 4 atoms) with a resulting coverage of 0.111 ML. For the Cu or Au monolayer, we used a 2×2 unit cell (64 atoms) but with 8 Cu or Au atoms on the surface resulting in a 0.5 ML coverage. In each case, a suitable Monkhorst–Pack of special k points has been used: $5 \times 5 \times 1$ for the 2×2 unit cell and $3 \times 3 \times 1$ for the 3×3 unit cell. The present models of supported Cu and Au nanoparticles are realistic enough to provide a meaningful comparison with experiment. In order to appropriately compare the chemical activity of the supported systems, DFT-based calculations were carried out for suitable models of the Cu(1 1 1)-, Cu(1 0 0)-, Au(1 1 1)-, and Au(1 0 0)-extended surfaces. For these surfaces, the slab was cut from the bulk using the calculated lattice parameter, a 3×3 unit cell was used with four atomic layers (36 metal atoms) and the two outermost ones completely relaxed. Here, it is important to mention that the Cu or Au atoms in the supported monolayer sit above the C atoms, and the C–C distances between next and next neighbors in TiC (3.066 and 4.337 Å) are sufficiently large to prevent any distortion thus not causing any stress due to lattice mismatch. Moreover, in the case of the Cu_4- and Au_4-supported particles, the interaction between either Cu or Au and C is large enough to maintain the structure avoiding clustering or sintering

In order to determine the lowest energy structures of the reactants and products of SO_2 and SO dissociation on all the systems described in the preceding paragraph, several geometry optimization calculations were carried out starting from different starting geometries. Once the final geometries were obtained for the SO_2 on Cu or Au/TiC(0 0 1) systems, a proper vibrational analysis has been used to characterize final geometries as minimum energy structures and the corresponding adsorption energies calculated as:

$$E_{ads} = -\left[E_{SO_2}(\text{ads on M/TiC}) - (E_{SO_2}(\text{gas}) + E_{M/TiC}(\text{clean}))\right] \quad (1)$$

where $E_{SO_2}(\text{gas})$ is the energy of the isolated SO_2 molecule; $E_{M/TiC}(\text{clean})$ is the total energy of the relaxed Cu or Au/TiC(0 0 1) surface, and $E_{SO_2}(\text{ads on M/TiC})$ is the energy SO_2 absorbed on either Cu/TiC(0 0 1) or Au/TiC(0 0 1) surface. Similar calculations were carried out for the adsorption and dissociation of SO_2 on the extended low-index Miller surfaces commented earlier. Transition state structures for SO_2 dissociation into SO + O and further dissociation of SO into S + O were located with the help of the dimer [30] algorithms as implemented in VASP and properly characterized by vibrational analysis. We already mentioned that, in all calculations, the supported particle geometry, the position of the S and O atoms, and the two upper atomic layer coordinates of the TiC substrate were fully relaxed. For the extended surfaces, the geometry of the adsorbed species and the two outermost atomic layers were always fully relaxed. However, in all cases, the vibrational analysis is restricted to the degrees of freedom of the S and O atoms. The activation energy barriers for SO_2 dissociation have been calculated as:

$$E_{act} = -[E_{OS\ldots O}(\text{TS on M/TiC}) - E_{SO_2}(\text{ads on M/TiC})] \quad (2)$$

where $E_{OS\ldots O}(\text{TS on M/TiC})$ is the energy of the transition state structure for SO_2 dissociation on SO + O and $E_{SO_2}(\text{ads on M/TiC})$ is as in Eq. (1). A similar expression is used to obtain the activation energy for the SO dissociation reaction into S + O and equivalent equations are used to obtain the activation energy for the same two corresponding elementary steps in the extended (0 0 1) and (1 1 1) surfaces.

Finally, the charge distributions were estimated by the method of Bader [31] for SO_2, SO, S and O adsorbed on the nanoparticles supported on TiC(0 0 1) as well as for the same species on the extended metal surfaces. Plots of the electron localization function [32] (ELF) have also been obtained to further analyze the effect of the underlying TiC on the electronic structure of the supported metal.

3. Results and discussion

3.1. Interaction of Cu and Au with TiC(0 0 1)

It is known that Cu and Au do not wet well stoichiometric TiC [9,10,33,34]. The images of scanning tunneling microscopy (STM) point to a lack of layer-by-layer growth, with the formation of two-dimensional (2D) and three-dimensional (3D) islands of the admetal over the carbide surface [9,10,34]. For very small coverages of the admetals ($\ominus$ <0.15 ML), the Au and Cu particles are mainly small (<1 nm in size) and flat. Fig. 1 displays the variation of the binding energy of the Cu $2p_{3/2}$ and Au $4f_{7/2}$ core-level peaks as a function of admetal coverage on TiC(0 0 1). Note that the data corresponding to Au on TiC have been published in a previous work [35] and are included here for the sake of comparison. At very small Au coverages, a binding energy of 84.2 eV was observed, and there was a monotonic decrease up to a value of ~83.8 eV at coverages above 0.5 ML. The final value is close to that seen in our instrument for bulk metallic gold. The positive shift (~0.35 eV) in the Au $4f_{7/2}$ peak at very low Au coverages could be due to a redistribution of charge around the adatoms [35]. This is in agreement with the modification of the line shape of the C(1s) peak in the presence of Au [35,36] and Cu. The electronic perturbation of the C(1s) induced by the presence of Au cannot be attributed to charge transfer effects since a Bader analysis [31] show that the Au atoms are almost neutral with a small negative charge (see Supplementary Information). In a previous work [35], the core-level shifts in Au/TiC(0 0 1) were attributed to a reduction in the repulsion between localized core electrons and valence electrons moving away from the C and Au centers, resulting in an effective decrease in the charge density around Au and C. It is likely that the same effect holds for the case of the Cu/TiC system where one sees a small positive binding energy shift of ~0.18 eV for the lowest coverage of the admetal. In addition, one must recall that while charge transfer may be the dominant effect responsible for core-level shift in many systems, other subtle physical mechanisms such as electric fields, atomic coordination, among others, do also contribute to the measured shift making the interpretation more difficult [37]. The data in Fig. 1 implies that there are electronic perturbations in the electronic structure of supported noble metal atoms, with the perturbations for Au being larger than for Cu.

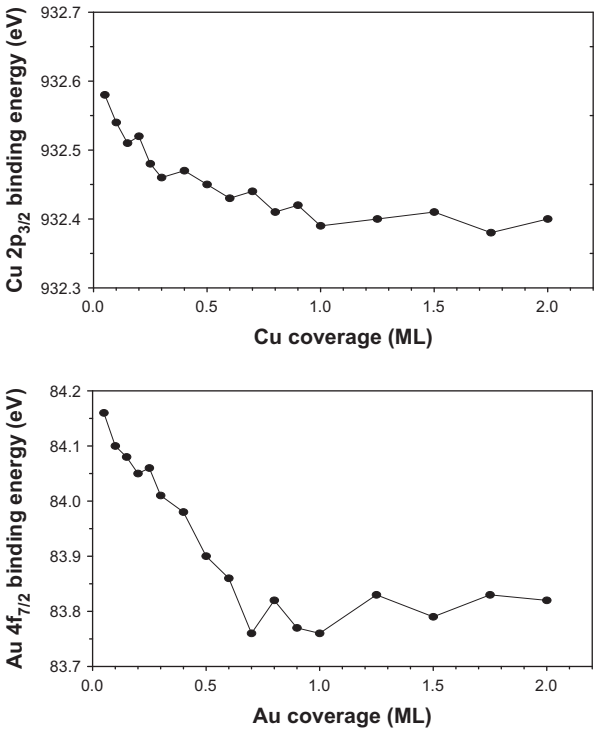

Fig. 1. Variation of the Cu $2p_{3/2}$ (top panel) and Au $4f_{7/2}$ (bottom panel) binding energy as a function of admetal coverage on TiC(0 0 1). The binding energies measured in our instrument for the Au $4f_{7/2}$ and Cu $2p_{3/2}$ peaks of the bulk metals are 83.8 and 932.4 eV, respectively. The photoemission data for the Au $4_{7/2}$ peak was obtained using a photon energy of 380 eV, while Mg K radiation was used to measure the position of the Cu $2p_{3/2}$ peak.

The top part of Fig. 2 displays electron-polarization function (ELF) [32] plots for Cu_4 and Au_4 on TiC(0 0 1). The corresponding results for supported monolayers are shown in the bottom part of the figure. In the case of Au_4/TiC(0 0 1) and $Au_{monolayer}$/TiC(0 0 1), the ELF maps show that there is a substantial concentration of electron located in the region outside the supported Au systems. A similar phenomenon is observed for the Cu_4/TiC(0 0 1) and $Cu_{monolayer}$/TiC(0 0 1) systems, but the magnitude of the electron polarization is not as large as seen for the supported Au_4 and $Au_{monolayer}$. The relatively large valence orbitals of gold favor a large electron polarization upon interaction of this admetal with TiC(0 0 1). Nevertheless, although a more detailed analysis of the ELF plots is required to achieve a quantitative interpretation, results in Fig. 2 are consistent with the photoemission results in Fig. 1 in the sense that both theory and experiment show significant electronic perturbations for small Cu and Au clusters in contact with TiC(0 0 1). On the basis of the charge polarization induced by the carbide substrate, one can expect important differences with respect to the chemical properties of bulk surfaces of Cu and Au. It is also important to note that, in addition to the electron polarization evidenced in the ELF plots, a Bader analysis of the

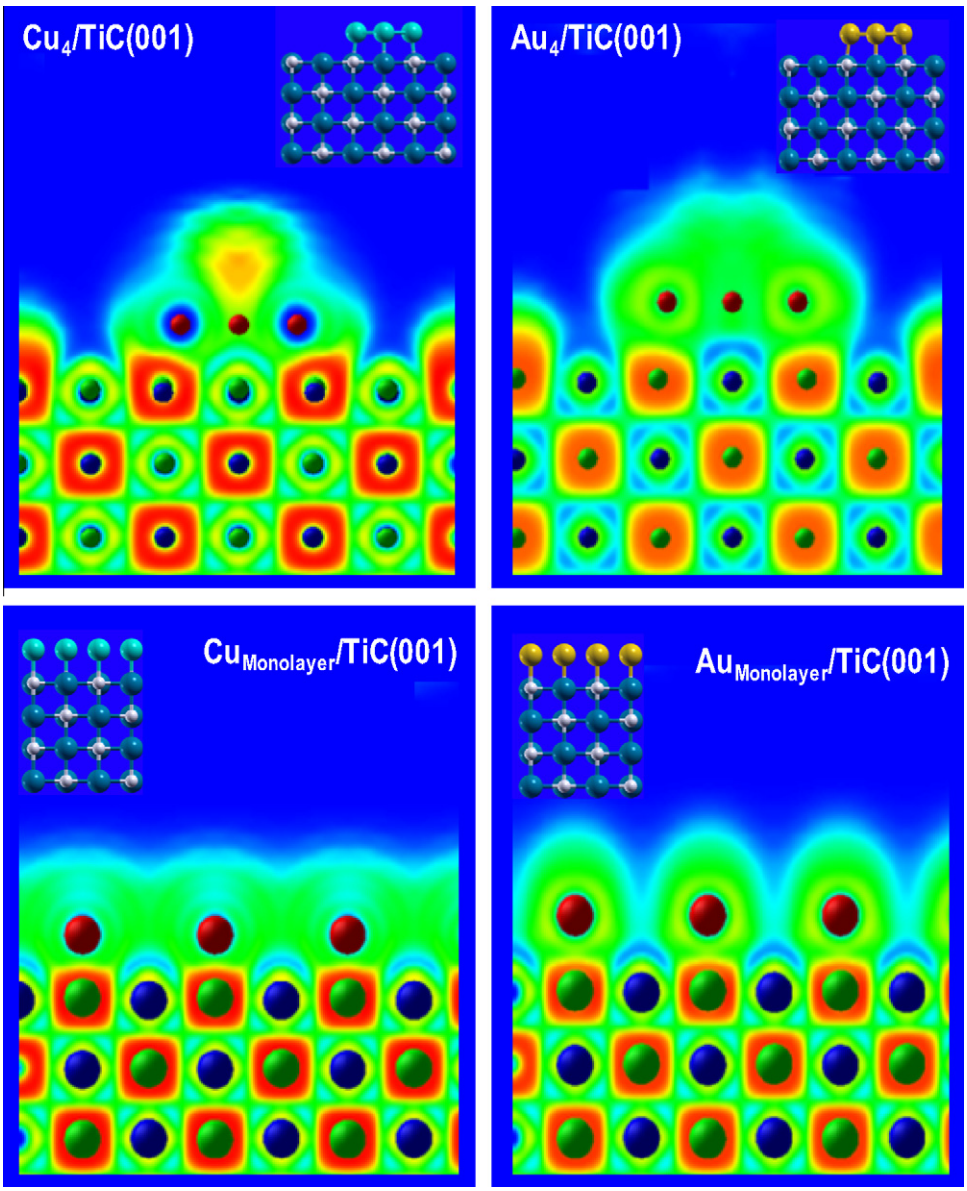

Fig. 2. Electron-polarization function plots for Cu_4 (top left) Au_4 (top right), $Cu_{monolayer}$ (bottom left) and $Au_{monolayer}$ (bottom right) supported on TiC(0 0 1). The metal atoms are adsorbed on C sites of the TiC(0 0 1) surface. The probability of finding electron pairs varies from 0 (blue color) to 1 (red color) .Thus, the green shape above the metal particle or monolayer denotes a substantial probability of electron pair localization. (For interpretation of the references to color in this figure legend, the reader is referred to the web version of this article.)

charge density finds a charge transfer from the TiC substrate to the atoms in Au_4 and Cu_4. For Cu_4/TiC(0 0 1), the average charge in the Cu atoms is of ~−0.17e, somewhat larger than the corresponding value for supported Au systems, which at most is ~−0.1e only [35].

3.2. Reaction of SO_2 with Cu/TiC(0 0 1) and Au/TiC(0 0 1): Photoemission studies

At the bottom of Fig. 3 is shown a S 2p spectrum acquired after dosing SO_2 to clean TiC(0 0 1). Dosing at 150 K prevents the adsorption of a physisorbed multilayer, and the features in the S 2p spectrum correspond to chemisorbed SO_2 species [19]. They match the binding energies for SO_2 adsorbed on carbides, oxides and metals [19]. When the SO_2/TiC(0 0 1) surface is heated from 150 to 300 K, top panel in Fig. 4, most (~70%) of the SO_2 desorbs intact and a small fraction undergoes full dissociation depositing S on the surface [19]. Thus, clean TiC(0 0 1) can be classified as a poor $DeSO_x$ material. This drastically changed after depositing Cu or Au on the carbide surface.

In Fig. 3, the deposition of Cu (0.1–0.2 ML) on SO_2/TiC(0 0 1) at 150 K induces the cleavage of the two S–O bonds in SO_2 and features for atomic S appear at 161–163 eV in the S 2p region [19]. Upon the deposition of the Cu, ~40% of the SO_2 present in the surface decomposed. This is quite remarkable because SO_2 does not decompose on Cu(1 0 0) or Cu(1 1 1) at 150 K [14,15,17]. For example, on Cu(1 1 1), significant dissociation of SO_2 is not seen up to a temperature near 250 K [17]. In the bottom panel of Fig. 4, we plot the evolution of SO_2 and S signals for a Cu/SO_2/TiC(0 0 1) system as a function of temperature. The 0.2 ML of Cu present on the surface dissociated most (~80%) of the adsorbed SO_2 at temperatures below 250 K. Furthermore, for the Cu/SO_2/TiC(0 0 1) system, we did not observe the formation of SO_3/SO_4 species that is a common feature for the disproportionation of SO_2 on Cu(1 0 0) or Cu(1 1 1) [14,15,17]. Therefore, the Cu ↔ TiC(0 0 1) interactions produce a

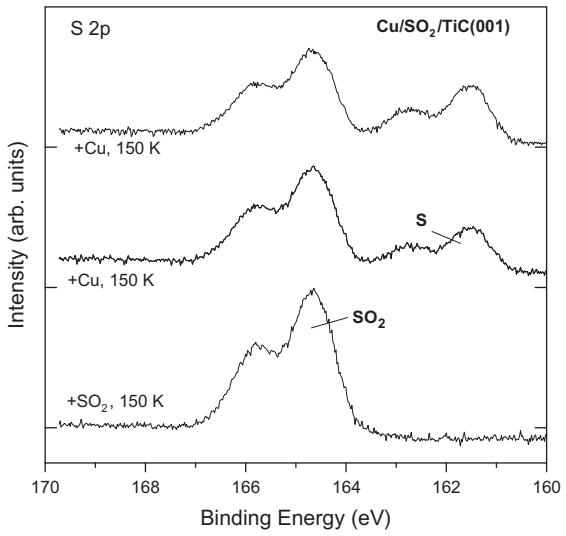

Fig. 3. S 2p core-level photoemission spectra for SO_2/TiC(0 0 1) and Cu/SO_2/TiC(0 0 1) surfaces. A saturation coverage of chemisorbed SO_2 was dosed to clean TiC(0 0 1) at 150 K and next 0.1 (middle curve) and 0.2 ML (top curve) of Cu were deposited on the TiC(0 0 1) surface. A photon energy of 380 eV was used to excite the electrons.

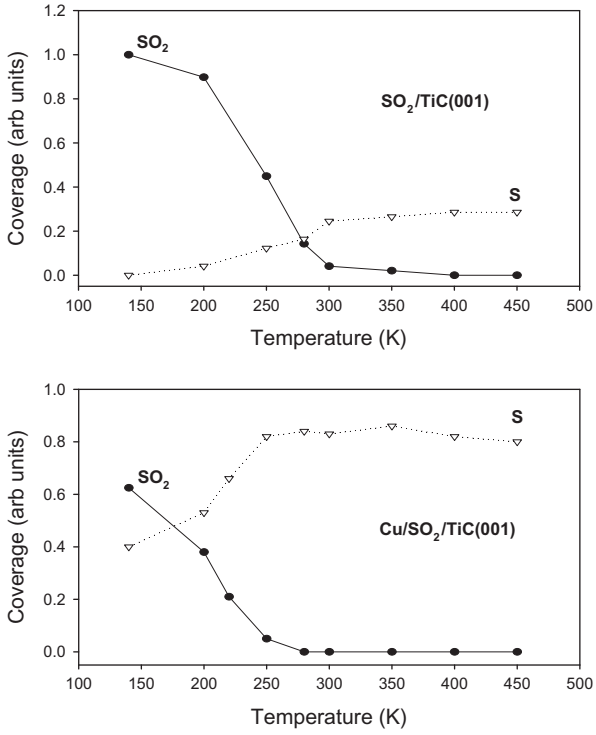

Fig. 4. Evolution of the SO_2 and S signals in SO_2/TiC(0 0 1), top panel, and Cu/SO_2/TiC(0 0 1), bottom panel, as a function of temperature. The amount of chemisorbed SO_2 initially adsorbed in these systems was the same. The TiC(0 0 1) was saturated with SO_2 at 150 K, with subsequent heating (top panel) or with deposition of Cu (0.2 ML) followed by heating (bottom panel).

system that has a $DeSO_x$ activity much higher than that of TiC(0 0 1) or extended surfaces of copper.

In general, we found that TiC(0 0 1) surfaces pre-covered with small amounts (<0.2 ML) of Cu or Au were quite efficient for the full dissociation of SO_2 at 200–300 K. SO_2 did not survive upon adsorption on Cu/TiC(0 0 1) and Au/TiC(0 0 1). Fig. 5 displays the amount of atomic sulfur deposited on Cu/TiC(0 0 1) and Au/

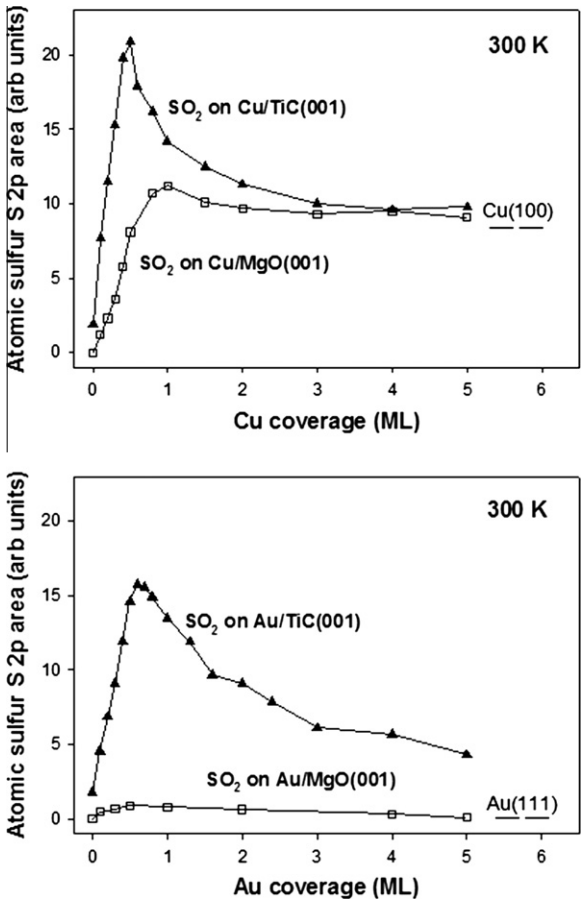

Fig. 5. S 2p areas measured for atomic S after dosing SO_2 (5L) to Cu/TiC(0 0 1) and Au/TiC(0 0 1) surfaces at 300 K. The dashed lines in the right-side of the figure denote the corresponding S 2p areas found after dosing SO_2 to Au (1 1 1) or a polycrystalline surface of Au (no activity in both cases) and Cu(1 0 0). For comparison, we also include the corresponding data for the adsorption of SO_2 on Cu/MgO(0 0 1) and Au/MgO(0 0 1) surfaces [5,38].

TiC(0 0 1) surfaces after dosing 5 L of SO_2 at 300 K. One can see that the coverage of the admetal drastically affects the $DeSO_x$ activity. Comparing to data of STM, [9,10] one can conclude that the highest chemical activity is seen for very small particles (<1 nm in size) of the admetals in close contact with the TiC(0 0 1) substrate. In Fig. 5, the dashed lines denote the amount of S deposited after dosing 5 L of SO_2 to polycrystalline gold (or Au(1 1 1)) and Cu(1 0 0) at room temperature. As mentioned earlier, extended gold surfaces do not have any $DeSO_x$ activity [8], and there is a tremendous enhancement in chemical activity after depositing small gold nanoparticles on TiC(0 0 1) [9,10]. Cu(1 0 0) is able to dissociate SO_2 [12,13,16], but if one normalizes the data in Fig. 5 (i.e. the signal for the deposited atomic S) by the number of Cu atoms present in the surface, it is clear that TiC(0 0 1) surfaces with small amounts (<0.5 ML) of Cu are much better $DeSO_x$ systems than Cu(1 0 0). In fact, for the same coverage of the admetal, Cu/TiC(0 0 1) always has a higher $DeSO_x$ activity than Au/TiC(0 0 1). This is quite a remarkable result since, opposite to Au, Cu is a cheap metal, and, therefore, one may attempt to prepare Cu/TiC catalysts to operate under more practical conditions.

In order to reinforce the conclusions above about the special role of the TiC support on changing the properties of the supported Cu and Au nanoparticles, we include in Fig. 5 the corresponding data for the deposition of Cu and Au nanoparticles on MgO(1 0 0) [5,38] since MgO is a common material used in $DeSO_x$ operations [2a,3a,5,11a]. The interactions of the admetals with MgO are not

as strong as those seen with TiC, and the Cu/MgO(0 0 1) and Au/MgO(0 0 1) systems do not match the $DeSO_x$ activity of either Cu/TiC(0 0 1) or Au/TiC(0 0 1). The deposition of Cu and Au on titania and ceria can lead to systems that are able to dissociate SO_2 but only when a substantial amount of O vacancies is introduced in these oxide supports [5]. From the O vacancies in titania and ceria, there is an electron transfer to Au and Cu that helps in the dissociation of the SO_2 molecule [5]. The electron polarization seen in Fig. 2 after setting Cu and Au clusters in contact with TiC(0 0 1) is a key to the high $DeSO_x$ activity found for the admetal/carbide systems. It must be pointed out that the Cu/TiC(0 0 1) or Au/TiC(0 0 1) systems were also very active for the dissociation of H_2S. These metal/carbide systems were able to catalyze the Claus reaction ($SO_2 + 2H_2S \rightarrow 3S + 2H_2O$) and the reduction of sulfur dioxide by CO ($SO_2 + 2CO \rightarrow 2CO_2 + S$) under high vacuum conditions. In the next section, we present a detailed theoretical study of the adsorption and dissociation of SO_2 on Cu/TiC(0 0 1) and Au/TiC(0 0 1) surfaces since these are perhaps the most important steps for obtaining an efficient $DeSO_x$ catalyst.

3.3. Reaction of SO_2 with Cu/TiC(0 0 1) and Au/TiC(0 0 1): Density functional studies

Not unexpectedly, the adsorption energy of SO_2 on the extended Au(1 1 1) and Au(1 0 0) surfaces is almost zero meaning that the contact time of this species with the extended gold surfaces will be too short to further react. Moreover, the calculated activation energy barriers exceed 2 eV, which is consistent with the inexistent $DeSO_x$ activity of extended Au surfaces. For the Cu(1 1 1) and Cu(1 0 0), the SO_2 adsorption energy is larger, 1.32 and 1.15 eV, respectively, indicating a possible larger activity toward SO_2 dissociation, which indeed is in agreement with experimental evidence that both Cu(1 0 0) and Cu(1 1 1) are able to dissociate SO_2 [12–16]. Still, we found that the activation energy for SO_2 dissociation on these two extended surfaces is still significant (1.13 and 0.93 eV, see Figs. S1-1 and S1-2) again in agreement with experimental evidence that these extended surfaces constitute poor $DeSO_x$ catalysts.

Next, we analyze in detail the energy profiles for the SO_2 dissociation reaction on the various model systems for Cu and Au supported on TiC. We start with the case of Au for which previous experimental and theoretical results have shown that, contrarily to extended surfaces, small Au nanoparticles supported on TiC(0 0 1) have a remarkable desulfurization activity [9,10]. Here, we present the detailed molecular mechanism for SO_2 dissociation on Au/TiC represented by two limiting situations, a Au_4 flat particle and an extended monoatomic Au layer, both supported on TiC(0 0 1). In principle, Au_4/TiC(0 0 1) is a good model to represent the small two-dimensional particles observed in STM experiments when low coverages of Au are deposited on TiC(0 0 1) [9,10] and one sees very high $DeSO_x$ activity. Figs. 6 and 7 provide the calculated energy profile for Au_4/TiC and $Au_{monolayer}$/TiC, respectively. These profiles give the adsorption energy of SO_2 and the activation energy for the dissociation of adsorbed SO_2 into SO + O, for the spillover of atomic O to the TiC surface and for subsequent dissociation of SO into S + O. Both Au/TiC systems exhibit a relatively low activation energy for SO_2 dissociation into SO + O, 0.32 eV in the case of supported Au_4 and 0.60 eV in the case of the supported monolayer. Moreover, spillover of atomic oxygen into the TiC(0 0 1) substrate appears to be favorable and the energy barrier for further dissociation of the SO molecule adsorbed on the Au-supported particle into adsorbed atomic S and O is also quite low, 0.54 and 0.74 eV for Au_4/TiC and $Au_{monolayer}$/TiC, respectively, indicating that complete dissociation may occur at quite low temperature as observed in our experiments. Note that the dissociation process is facilitated by the rather large adsorption energy of SO_2 on both Au/TiC model systems. This prediction is in agreement with experimental findings in previous [9] and present experiments that evidence the presence of atomic sulfur upon dosing SO_2 on the Au/TiC(0 0 1) system (Figs. 4 and 5).

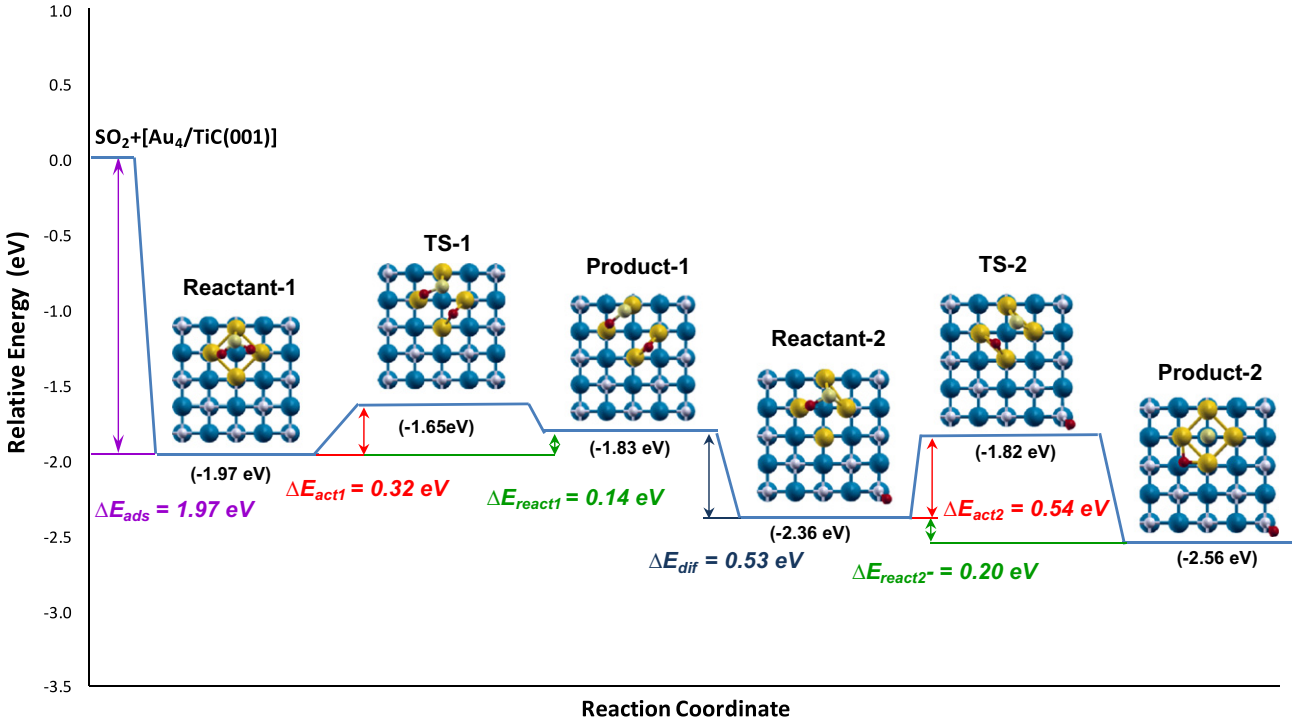

Fig. 6. Energy profile for SO_2 dissociation on the Au_4/TiC(0 0 1) model system. The different elementary steps indicated are SO_2 dissociation into SO + O, spillover of O from the metal supported particles to TiC and subsequent SO dissociation into S + O. Large blue spheres stand for Ti, small white for C, large yellow for Au, small light yellow for S and small red for O. (For interpretation of the references to color in this figure legend, the reader is referred to the web version of this article.)

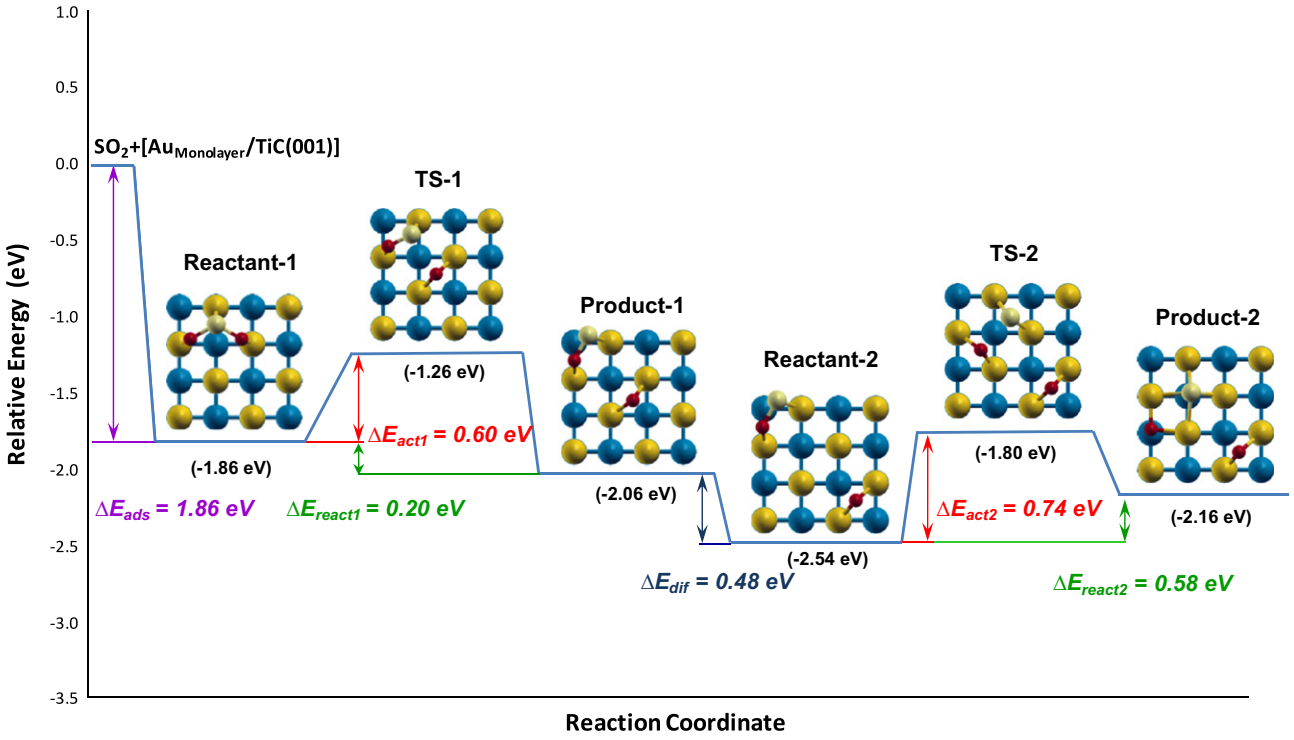

Fig. 7. Energy profile for SO_2 dissociation on the $Au_{monolayer}/TiC(0\,0\,1)$ model system. The adsorbed SO_2 molecule dissociates into SO and O with subsequent SO dissociation into S + O. Color code is as in Fig. 6. (For interpretation of the references to color in this figure legend, the reader is referred to the web version of this article.)

Let us turn our attention to the results corresponding to the Cu_4/TiC and $Cu_{monolayer}/TiC$ systems that are summarized in Figs. 8 and 9. The adsorption energies of SO_2 on $Cu_4/TiC(0\,0\,1)$, 2.72 eV, and $Cu_{monolayer}/TiC(0\,0\,1)$, 3.67 eV are much larger than those calculated on Cu(1 1 1), 1.32 eV (Fig. S1-2), and Cu(1 0 0), 1.15 eV (Fig. S1-1). In fact, the energy released during the adsorption of SO_2 is so larger that it can easily help to overcome the activation barriers associated with the cleavage of the S–O bonds. In the cases of $Cu_4/TiC(0\,0\,1)$ and $Cu_{monolayer}/TiC(0\,0\,1)$, the decrease in activation energy with respect to the extended copper surface is not as dramatic as in the case of Au, but it has some particularities that may render this system even more attractive than Au/TiC, especially for practical purposes. In fact, the activation energy for the dissociation of SO_2 into SO + O on Cu_4/TiC and $Cu_{monolayer}/TiC$ are 0.76 and 0.64 eV, respectively. The first one is somewhat smaller than the calculated energy barrier for the extended Cu surfaces – 1.13 and 0.93 eV for Cu(0 0 1) and Cu(1 1 1), respectively – but the second one is sensibly smaller, indicating that flat Cu particles supported on TiC should be very active toward SO_2 dissociation, a prediction that is fully supported by the experiments reported in the previous section. Note that the difference between the energy profiles corresponding to SO_2 dissociation on Cu_4/TiC and $Cu_{monolayer}/TiC$ are indicate that flat particles with size intermediate between these two limiting situations are likely to be the most active.

For the second dissociation step, SO into S + O, the calculated energy barriers on Cu_4/TiC and $Cu_{monolayer}/TiC$ are 0.31 and 0.27 eV, respectively. Note that these are significantly smaller than the corresponding values for the Au_4/TiC and $Au_{monolayer}/TiC$ models that are 0.54 and 0.74 eV, respectively. Hence, the Au/TiC system seems to be appropriate to dissociate SO_2 into SO + O whereas the Cu/TiC is more active toward SO dissociation. At this point, one may even speculate that a system containing supported Cu and Au small nanoparticles on TiC(0 0) would provide a better $DeSO_x$ catalyst. Another particularity of the Cu/TiC system compared to the Au/TiC counterpart is the much larger adsorption energy of SO_2 on $Cu/TiC(0\,0\,1)$, which easily provides the energy necessary to overcome the barriers for the breaking of the S–O bond. This explains the observed activity of the Cu/TiC system as evidenced in Figs. 3 and 5. As in the case of Au/TiC, the metal ↔ C interactions evidenced in the ELF plots in Fig. 2 are responsible for the predicted and observed catalytic activity of these systems, especially when compared with the activity of similar particles supported on $MgO(0\,0\,1)$, see Fig. 5.

Interestingly, although $Cu/TiC(0\,0\,1)$ interacts stronger with SO_2 than $Au/TiC(0\,0\,1)$, the magnitude of the change in reactivity when going from bulk to nanoparticles supported on $TiC(0\,0\,1)$ is larger for Au. In fact, while the Au(1 1 1) or Au(1 0 0) surfaces are useless for the dissociation of SO_2, the $Au/TiC(0\,0\,1)$ works well. The large polarization seen in Fig. 2 for Au can explain this. The enhancement in reactivity with respect to Cu(1 1 1) or Cu(1 0 0) is less dramatic but yet quite important. The high price of Au prevents its use on a large scale in industrial applications. On the other hand, the Cu/TiC system, while being extremely active (Fig. 5), has also the advantage of the relatively low cost of Cu making it very attractive as a potential candidate for $DeSO_x$ catalysts.

4. Summary and conclusions

In this work, experiments and density functional calculations on Au/TiC and Cu/TiC model systems are reported, which evidence that these two systems are very active for the dissociation of the SO_2 molecule and that the origin of the activity lies on the interaction between the C atoms of the substrate and the metal atoms of the supported particle, which result in a large polarization of its electron density. Both experiments and theory indicate that the Cu/TiC system is more active toward SO_2 dissociation although the activity of the Au/TiC is also remarkable. The higher energy barriers predicted for the dissociation of SO_2 on Cu/TiC system

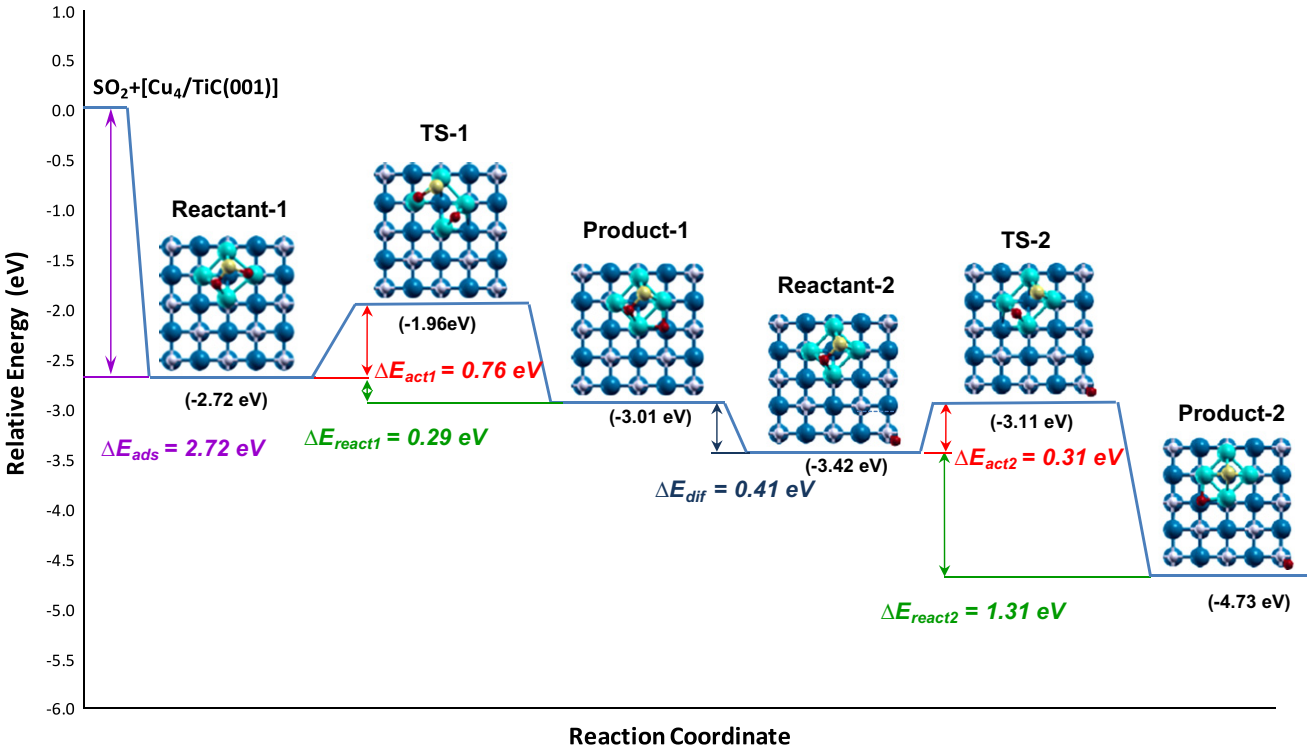

Fig. 8. Energy profile for SO_2 dissociation on the Cu_4/TiC(0 0 1) model system. The different elementary steps indicated are SO_2 dissociation into SO + O, spill over of O from the metal supported particles to TiC and subsequent SO dissociation into S + O. Large blue spheres stand for Ti, small white for C, medium light blue for Cu, small light yellow for S and small red for O. (For interpretation of the references to color in this figure legend, the reader is referred to the web version of this article.)

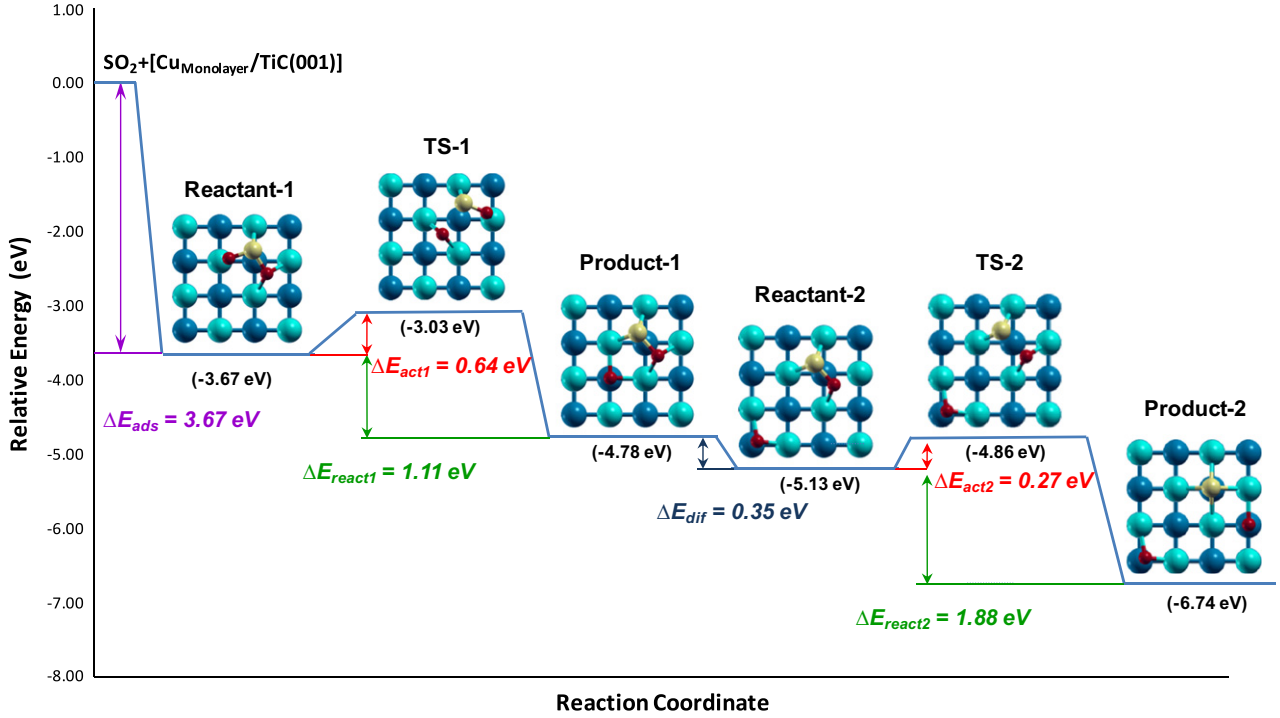

Fig. 9. Energy profile for SO_2 dissociation on the $Cu_{monolayer}$/TiC(0 0 1) model system. The adsorbed SO_2 molecule dissociates into SO and O with subsequent SO dissociation into S + O. Color code is as in Fig. 8. (For interpretation of the references to color in this figure legend, the reader is referred to the web version of this article.)

can be easily overcome thanks to the rather large adsorption energy of SO_2, thus explaining the $DeSO_x$ activity found in the present experiments. In Cu/TiC, one has a highly efficient and non-expensive system for the destruction of SO_2. Such system is also able to perform the dissociation of H_2S and can catalyze the Claus reaction ($SO_2 + 2H_2S \rightarrow 3S + 2H_2O$) and the reduction of sulfur dioxide by CO ($SO_2 + 2CO \rightarrow 2CO_2 + S$) under high vacuum conditions. This opens the door toward a new family of $DeSO_x$ catalysts, and addi-

tional tests with realistic industrial conditions are necessary. Moreover, the fact that Au/TiC facilitates the SO_2 dissociation into SO + O and that Cu/TiC is more active for the SO dissociation into S + O together with recent advances into the preparation of these systems [34] points the way toward bifunctional $DeSO_x$ catalysts consisting of mixtures of Cu and Au on TiC(0 0 1).

Acknowledgments

The authors are grateful to K. Nakamura (Tokyo Institute of Technology) for facilitating the TiC(0 0 1) crystal on which the experiments described in this article were performed. The research carried out at Brookhaven National Laboratory was supported by the US Department of Energy (Chemical Sciences Division, DE-AC02-98CH10886). The National Synchrotron Light Source is supported by the Divisions of Chemical and Materials Science of the US Department of Energy. L.F. is grateful to ICyTDF for a Postdoctoral Fellowship and F.I. acknowledges financial support through Spanish MICINN grant FIS2008-02238/FIS, through the "2009 ICREA Academia" prize for excellence in research and, in part, from Generalitat de Catalunya grants 2009SGR1041 and XRQTC. Generous allocation of computational time on the *Marenostrum* supercomputer of the Barcelona Supercomputing Center is gratefully acknowledged.

Appendix A. Supplementary material

Supplementary data associated with this article can be found, in the online version, at doi:10.1016/j.jcat.2011.02.004.

References

[1] D. Vallero, Fundamentals of Air Pollution, fourth ed., Academic Press, NewYork, 2007.
[2] (a) A. Pieplu, O. Saur, J.-C. Lavalley, O. Legendre, C. Nedez, Catal. Rev. Sci. Eng. 40 (1998) 409;
(b) A. Tshope, W. Liu, M. Flytzani-Stephanopoulos, J.Y. Ying, J. Catal. 157 (1995) 42;
(c) M.T. Flytzani-Stephanopoulos, Y. Li Zhu, Catal. Today 62 (2000) 145.
[3] (a) C.D. Cooper, F.C. Alley, Air Pollution Control, third ed., Waveland Press, New York, 2002;
(b) D.D. Beck, J.W. Sommers, C.L. DiMaggio, Appl. Catal. B 11 (1997) 273;
(c) S. Livraghi, M.C. Paganini, E.J. Giamello, Mol. Catal. A: Chem. 322 (2010) 39.
[4] J.G. Speight, The Chemistry and Technology of Petroleum, second ed., Dekker, New York, 1991.
[5] J.A. Rodriguez, P. Liu, M. Pérez, G. Liu, J. Hrbek, J. Phys. Chem. A 114 (2010) 3802.
[6] (a) H.H. Hwu, J.G. Chen, Chem. Rev. 105 (2005) 185;
(b) E. Furimsky, Appl. Catal. A 240 (2003) 1;
(c) S.T. Oyama, Catal. Today 15 (1992) 179.
[7] (a) J.A. Rodriguez, J. Dvorak, T. Jirsak, J. Phys. Chem. B 104 (2000) 11515;
(b) J.A. Rodriguez, J. Liu, Y. Takahashi, K.F. Viñes, F. Illas, Top. Catal. 53 (2010) 393.
[8] G. Liu, J.A. Rodriguez, J. Dvorak, J. Hrbek, T. Jirsak, Surf. Sci. 505 (2002) 295.
[9] J.A. Rodriguez, P. Liu, F. Viñes, F. Illas, Y. Takahashi, K. Nakamura, Angew. Chem. Int. Ed. 47 (2008) 6685.
[10] J.A. Rodriguez, P. Liu, F. Viñes, F. Illas, Y. Takahashi, K. Nakamura, J. Am. Chem. Soc. 131 (2009) 8592.
[11] (a) K.C. Hass, W.F. Schneider, Phys. Chem. Chem. Phys. 1 (1999) 639;
(b) G. Centi, N. Passarini, S. Perathoner, A. Riva, Ind. Eng. Chem. Res. 31 (1992) 1947.
[12] J. Ahner, H.-W. Wassmuth, Surf. Sci. 287/288 (1993) 125.
[13] T. Nakahashi, S. Terada, T. Yokoyama, H. Hamamatsu, Y. Kitajima, M. Sakano, F. Matsui, T. Ohta, Surf. Sci. 373 (1997) 1.
[14] M. Polčik, L. Wilde, J. Haase, Phys. Rev. B 57 (1998) 1868.
[15] G.J. Jackson, S.M. Driver, D.P. Woodruff, N. Abrams, R.G. Jones, M.T. Butterfield, M.D. Crapper, B.C.C. Cowie, V. Farmoso, Surf. Sci. 459 (2000) 231.
[16] J.A. Rodriguez, J.M. Ricart, A. Clotet, F. Illas, J. Chem. Phys. 115 (2001) 454.
[17] M. Polčik, L. Wilde, J. Haase, B. Brena, D. Cocco, G. Comelli, G. Paolucci, Phys. Rev. B 53 (1996) 13720.
[18] (a) H. Sellers, E. Shustorovich, J. Mol. Catal. A: Chem. 119 (1997) 367;
(b) H. Sellers, E. Shustorovich, Surf. Sci. 356 (1996) 209.
[19] J.A. Rodriguez, P. Liu, J. Dvorak, T. Jirsak, J. Gomes, Y. Takahashi, K. Nakamura, Surf. Sci. 543 (2003) L675.
[20] P.P. Frantz, Didziulis, Surf. Sci. 412/413 (1998) 384.
[21] (a) J.A. Rodriguez, G. Liu, T. Jirsak, J. Hrbek, Z. Chang, J. Dvorak, A. Maiti, J. Am. Chem. Soc. 124 (2002) 5242;
(b) X. Zhao, J. Hrbek, J.A. Rodríguez, M. Pérez, Surf. Sci. 600 (2006) 229.
[22] J.A. Rodriguez, M. Kuhn, Surf. Sci. 330 (1995) L657.
[23] J. Perdew, Y. Wang, Phys. Rev. B 45 (1992) 13244.
[24] P.E. Blochl, Phys. Rev. B 50 (1994) 17953.
[25] G. Kresse, D. Joubert, Phys. Rev. B 59 (1999) 1758.
[26] G. Kresse, J. Hafner, Phys. Rev. B 47 (1993) 558.
[27] G. Kresse, J. Furthmüller, Phys. Rev. B 54 (1996) 11169.
[28] H.J. Monkhorst, J.D. Pack, Phys. Rev. B 13 (1976) 5188.
[29] F. Viñes, C. Sousa, P. Liu, J.A. Rodriguez, F. Illas, J. Chem. Phys. 122 (2005) 174709.
[30] G. Henkelman, H. Jónsson, J. Chem. Phys. 111 (1999) 7010.
[31] (a) R.F.W. Bader, Atoms in Molecules: A Quantum Theory, Oxford Science, Oxford, UK, 1990;
(b) R. Bader, Chem. Rev. 91 (1991) 893.
[32] B. Silvi, A. Savin, Nature 371 (1994) 683.
[33] S.V. Dudiy, B.I. Lundqvist, Phys. Rev. B 69 (2004) 125421.
[34] (a) L.K. Ono, D. Sudfeld, B. Roldan Cuenya, Surf. Sci. 600 (2006) 5041;
(b) A. Naitabdi, L.K. Ono, B. Roldan Cuenya, Appl. Phys. Lett. 89 (2006) 043101.
[35] J.A. Rodriguez, F. Viñes, F. Illas, P. Liu, Y. Takahashi, K. Nakamura, J. Chem. Phys. 127 (2007) 211102.
[36] W.F. Egelhoff, Surf. Sci. Rep. 6 (1987) 253.
[37] P.S. Bagus, F. Illas, G. Pacchioni, F. Parmigiani, J. Electr. Spectrosc. Relat. Phenom. 100 (1999) 215.
[38] X. Zhao, J. Hrbek, J.A. Rodriguez, M. Pérez, Surf. Sci. 600 (2006) 229.